Geoderma 409 (2022) 115630

Contents lists available at ScienceDirect

Geoderma

journal homepage: www.elsevier.com/locate/geoderma

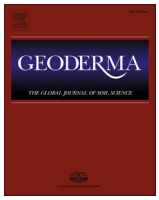

Estimating soil water suction from texture, bulk density and electrical resistivity

Lin Liu [a], Yili Lu [a], Yongwei Fu [b], Robert Horton [c], Tusheng Ren [a,*]

[a] College of Land Science and Technology, China Agricultural University, Beijing 100193, China
[b] Department of Crop and Soil Sciences, North Carolina State University, Raleigh 27695, NC, USA
[c] Department of Agronomy, Iowa State University, Ames 50011, IA, USA

ARTICLE INFO

Handling Editor: Morgan Cristine L.S.

Keywords:
Soil water suction
Soil water retention curves
Soil electrical resistivity
Formation factor

ABSTRACT

Information on soil water suction (h) is essential to study water flow and solute transport in soils, and to understand engineering behaviors of unsaturated soils. Due to limited availability of field methods that can accurately measure h, numerous studies have been performed to estimate h from more readily available soil properties. In this study, a new relationship between h and soil electrical resistivity (ρ), developed from the Gardner water retention model and Archie's second law, was used to estimate h values lower than the air entry value and a formation factor (expressed on log-scale) less than 1. The two model parameters (A and B), which are functions of soil texture and bulk density, were obtained by fitting the model to ρ and h data measured on soil columns of eight textures and various bulk densities. Laboratory and field evaluations with independent h and ρ data showed that the model estimated h values agreed well with the measured values, with root mean square errors less than 0.85 kPa. The model provides a new opportunity to evaluate in situ h dynamics and study coupled transport of water and solutes in the field.

1. Introduction

Measurements of soil water suction (h) are essential for studying water flow and solute transport in soils, and for understanding engineering behaviors of unsaturated soils (Karup et al., 2017). Accurate h values are also indispensable prerequisites for solving unsaturated soil mechanics problems (Pham and Fredlund, 2008; Perkins, 2011).

It usually requires more than one technique to measure h values over the entire water content range. A laboratory sandbox apparatus can impose matric suction (equivalent to h) on soil samples in the range of 0 to 10 kPa (Gupta and Larson, 1979; Romano et al., 2002), and the pressure plate extractor typically operates in the range of 100 to 1500 kPa (Richards, 1965; Dane and Hopmans, 2002). The pressure plate method, however, is time-consuming and susceptible to errors of poor soil-plate contact, low ceramic plate conductance, and soil volume change in the dry range (Bittelli and Flury, 2009). Tensiometers are one of the few sensors that are capable of directly measuring h under field conditions. However, the limited range of typical tensiometers (<100 kPa) restricts extensive applications of these sensors (Tian et al., 2018). Heat dissipation sensors determine water content of a ceramic buried in the soil indirectly from measured thermal conductivity, which is then translated into h using the water retention characteristic of the ceramic disc (Zhang et al., 2011). These sensors require individual calibration to provide reliable h information.

Although closed-form parametric models for soil water retention curves (SWRCs), which relate soil water content (θ) with h, can be applied to estimate continuous h values, they require several equilibrium h-θ measurements to characterize the entire SWRC (Naveed et al., 2012). Several pedotransfer functions (PTFs) have been developed to estimate SWRCs from easily accessible soil parameters such as particle size distribution (PSD), bulk density (BD), and organic matter (OM) content (Wösten et al., 1999; Schaap et al., 1998, 2000; Børgesen et al., 2008; Weynants et al., 2009). The performance of the PTFs depends strongly on the number and range of datasets that are used for their derivation and evaluation. Additionally, errors with the PTFs often arise because of the simplified treatment of the soil pore systems (Mohammadi and Vanclooster, 2011).

In porous media, water flow and electrical current are closely-related processes. This is caused by the fact that both water flow and electrical current transmission in soils occur mainly in the liquid phase, and the two processes are determined by similar soil parameters, e.g., texture, porosity (n), pore tortuosity, and θ (Vita et al., 2012; Piegari et al., 2013). In soils, electrical current transmission is expressed

* Corresponding author.
E-mail address: tsren@cau.edu.cn (T. Ren).

https://doi.org/10.1016/j.geoderma.2021.115630
Received 31 July 2021; Received in revised form 10 November 2021; Accepted 21 November 2021
Available online 30 November 2021

List of symbols

A, B	new model parameters
a, b	Gardner model parameters
d, m, c	parameters of Archie's second law
BD	soil bulk density (Mg m^{-3})
f_{cl}, f_{si}, f_{sa}	clay, silt, and sand fractions in a soil
h	soil water suction (kPa)
n	porosity
S	degree of saturation
S_e	effective saturation
w	phase exponent of pore water
α, β, l, p	parameters in Fu et al. (2021a) model
θ	soil water content (m^3 m^{-3})
θ_r	residual water content (m^3 m^{-3})
θ_s	saturated water content (m^3 m^{-3})
ρ	soil electrical resistivity (Ω m)
ρ_r	formation factor
ρ_w	soil electrical resistivity of pore water (Ω m)
σ	soil electrical conductivity (dS m^{-1})
σ_{dry}	electrical conductivity of dry soil (dS m^{-1})
σ_{res}	electrical conductivity of soil at residual water content (dS m^{-1})
σ_s	electrical conductivity of soil solids (dS m^{-1})
σ_{sat}	electrical conductivity of saturated soil (dS m^{-1})

mathematically with Ohm's law, which takes a form similar to that of Darcy's law for describing water flow.

Inspired by the analogy between soil water flow and electrical current in soils, researchers have examined the relations between hydraulic and electrical properties, for example, between soil hydraulic conductivity and apparent electrical conductivity (σ) for saturated porous media (Urish, 1981; Purvance and Andricevic, 2000; Slater and Lesmes, 2002). Doussan et al. (2009) extended the hydraulic-electrical conductivity relationship to unsaturated porous media by using the permeability-formation factor equation proposed by Katz and Thompson (1986) and converting the characteristic length scale to h using the capillary equation. Niu et al. (2015) developed a theoretical hydraulic conductivity-electrical conductivity relationship based on the bundle of capillary tubes model to fit the tortuosity factor in the Mualem-van Genuchten model (van Genuchten, 1980), which ignored the irreducible water content in porous materials and the bypass flow between neighboring capillary tubes.

The similarities between soil hydraulic and electrical properties make it appealing to relate hydraulic variables (e.g., h) to proxy and more readily measurable electrical properties. Because soil electrical resistivity (ρ, equals to 1/σ), which reflects the mobility of electrons in soils, can be monitored easily with techniques such as time domain reflectometry (TDR), it is an appropriate candidate to estimate the field dynamics of h (Sudduth et al., 2005; Doussan and Ruy, 2009; Stadler et al., 2015). However, due to the complexity of soil constituents, their differences in the ability to conduct electricity, the variability of electrical pathways, variable salt concentrations, and temporal dynamics of θ, the ρ values can vary over several orders of magnitude (Friedman, 2005; Pozdnyakov et al., 2006; Al-Moadhen, 2019), making it difficult to develop theoretical ρ models. As a result, the majority of ρ models are established empirically based on the assumption that the ρ magnitude of a bulk soil is governed by three pathways, i.e., the liquid conductance pathway, the solid conductance pathway, and the solid–liquid conductance pathway (Rhoades et al., 1989). A well-known ρ model is Archie's second law, which describes ρ as a power function of porosity and degree of saturation for unsaturated rocks and sandy soils (Archie, 1942).

Several studies have addressed the effects of varying water retention capacity on ρ under low and high θ ranges and proposed exponential relationships between ρ and θ (e.g., Pozdnyakov et al., 2006). Vita et al. (2012) performed geophysical and geotechnical laboratory analyses on pairs of pyroclastic samples collected from the same sites in an area susceptible to debris-flow landslides, and developed a direct positive relationship between ρ and h for the investigated ash-fall soil horizons. Based on the Vita et al. (2012) study, Piegari et al. (2013) proposed a ρ and h relationship for pyroclastic samples by combining the van Genuchten model and Archie's second law. This relationship includes four empirical parameters fitted to h-θ and ρ-θ curves, thus it lacks the ability to estimate unknown h or ρ values based on measured values of one or the other. Fu et al. (2021a) presented an approach to estimate the van Genuchten parameters from the entire ρ-θ curve, BD and soil texture based on the Mualem and Friedman (1991) model. Independent validation results showed that their approach performed well but had some limitations, such as relatively large estimation errors for soils with large BD values and at θ near full saturation. Few studies focused on estimating h values from measured values of ρ. If a universal h-ρ relationship could be established, then h values could be estimated from readily determined ρ values.

In this study, we developed an empirical h and ρ model by combining Archie's second law on electrical resistivity and the Gardner (1970) SWRC model. Laboratory and field measurements of h, ρ, and other soil physical properties were used to establish the h-ρ relationship, which was then evaluated with independent datasets.

2. Soils and experimental measurements

Laboratory and field experiments were performed to collect ρ and h data under various conditions covering a range of soil textures, BD, and θ. Table 1 lists the physical characteristics of the 11 soils examined, with sand content ranging from 0.18 to 0.94 g g^{-1} and clay content ranging from 0.05 to 0.31 g g^{-1}. For laboratory studies, the soil samples were air-dried, ground, and sieved through a 2-mm screen. Soil PSD was determined with the pipette method (Gee and Or, 2002), soil OM content was measured using the Walkley-Black titration method (Nelson and Sommers, 1982), and soil particle density was determined with the pycnometer method (Flint and Flint, 2002).

Simultaneous θ, ρ and h measurements were made on repacked samples during drying processes (Experiment 1), on repacked samples at various water contents (Experiment 2), and in the field during a maize growing season (Experiment 3). Data from soils 1–8 were used to establish the model, and data from soils 9, 10, and 11 were used to validate the model.

2.1. Experiment 1: sequential measurements on repacked soil samples during drying

Sequential ρ and h measurements were obtained on soils 1–6 during a soil drying period. The soil samples, which had passed through a 2-mm sieve, were repacked at desired BD values and θ values in cylinders (100-mm inner diameter and 100-mm in height) at room temperature (25 ± 1°C). A 3-needle TDR sensor (with 70-mm needle length, 2-mm needle diameter, and 10-mm needle-to-needle spacing) and a micro-tensiometer (25.4 mm long and 6.7 mm in diameter) equipped with a pressure transducer (Soil Measurement System, Tucson, AZ) were inserted horizontally into the soil column through pre-drilled holes at a distance of about 50 mm from the column surface. The soil columns were slowly saturated with distilled water, and then allowed to dry by evaporating water from the open top end exposed to the atmosphere. During the evaporation periods, a datalogger (model CR1000, Campbell

Table 1
The fractions of soil solids, organic matter (OM) content, bulk density (BD), particle density (ρ_s), and water content (θ) for the soils included in the study. Experiment 1 was conducted on repacked samples during drying processes, Experiment 2 was performed on repacked samples at various water contents, and Experiment 3 was performed in the field during a maize growing season.

	Soil ID	Texture	Fractions of soil solids			OM	BD	ρ_s	θ
			2–0.05 mm	0.05–0.002 mm	<0.002 mm				
			g g^{-1}			%	Mg m^{-3}	Mg m^{-3}	m^3 m^{-3}
Experiment 1	1	sand	0.94	0.01	0.05	0.90	1.58	2.66	0.06–0.28
	2	loamy sand	0.80	0.12	0.08	–	1.57	2.65	0.12–0.33
	3	sandy loam	0.70	0.23	0.07	0.86	1.40	2.69	0.14–0.43
	4	sandy loam	0.55	0.33	0.12	0.65	1.30	2.65	0.14–0.45
	5	clay loam	0.32	0.38	0.30	0.27	1.20	2.69	0.20–0.47
	6	silt loam	0.18	0.64	0.18	1.24	1.30	2.69	0.25–0.48
Experiment 2	7	silt loam	0.21	0.67	0.12	–	1.25	2.65	0.17–0.59
	8	clay loam	0.24	0.49	0.27	–	1.20	2.65	0.21–0.60
	9	sand	0.83	0.11	0.06	–	1.55, 1.60, 1.70	2.65	0.07–0.37
	10	silt loam	0.27	0.50	0.23	–	1.35, 1.45, 1.55	2.65	0.15–0.43
	11	clay loam	0.24	0.45	0.31	3.56	1.20, 1.30, 1.40	2.65	0.14–0.44
Experiment 3	11	clay loam	0.24	0.45	0.31	3.56	1.13	2.65	0.12–0.47

Scientific Inc., Logan, UT) recorded the signals from a TDR device and pressure transducers hourly until there were no obvious changes in the signals. The approaches for determining ρ and θ from TDR signals were reported by Heimovaara et al. (1995) and Ren et al. (1999), respectively. The voltage signals from the pressure transducer changed linearly with *h*. Refer to Zhang et al. (2017) for details on pressure transducer calibration to obtain the conversion equation between *h* and voltage signals. Following the evaporation period, gravimetric θ and BD values were determined by oven drying the soil cores at 105℃ for 24 h.

2.2. Experiment 2: individual measurements on repacked soil samples at various θ values

For soils 7–11, laboratory ρ and *h* measurements were made on soil cores (50 mm inner diameter and 50 mm in height) that were repacked at selected BD and θ values. Three replicated cores were prepared at each θ and BD combination. The soil columns were saturated slowly with distilled water, and then used for SWRC measurements in a sand box (with *h* values of 0.5, 0.75, 1.5, 4, 6, and 8 kPa) and a pressure plate apparatus (with *h* values of 10, 30, 70, 100, 300, and 500 kPa). After equilibration at a specific *h*, the sample mass was recorded, and ρ and θ were measured with the TDR technique. Briefly, a TDR sensor (45 mm long, 2 mm in diameter, and 8 mm needle-to-needle spacing) was inserted into each soil column vertically from the soil surface, TDR measurements were completed with a TDR200 system (Campbell scientific Inc., Logan, UT), and ρ and θ were estimated following Heimovaara et al. (1995) and Ren et al. (1999). Finally, the samples were oven-dried at 105℃ for 48 h to determine the dry mass.

2.3. Experiment 3: field measurements

Fields measurements were performed on a clay loam soil (soil 11) at the Lishu Experimental Station of China Agricultural University (43°16′ N, 124°26′ E), located in Lishu County, Jilin Province, China. To facilitate sensor installation, a small trench (about 150 mm long, 150 mm wide, and 150 mm deep) was made, and two TDR sensors (70 mm long, 2 mm in diameter, and 10 mm needle-to-needle spacing) were pushed horizontally into the soil at depths of 50 mm and 100 mm. Soil suction sensors (TensioMark, ecoTech Umwelt-Meßsysteme, GmbH, Bonn, Germany, 130-mm long, 20-mm wide, and 7-mm thick) were also installed at the 50- and 100-mm depths (but 50-mm away from the TDR sensors) to monitor the dynamics of *h*. The TensioMark sensors were covered with wet native soils before installation, and then inserted diagonally into a pre-made slot at the desired depths. A TDR200 system, which was controlled with a datalogger (model CR3000, Campbell Scientific Inc., Logan, UT), measured the θ and ρ values every 60 min. The TensioMark sensors were controlled with a datalogger (SDI-12, enviLog, Germany) via an SDI-12-multiple socket. Finally, undisturbed soil columns were collected near by the TensioMark sensors with ring samplers (50-mm in diameter and 50-mm high) at the 50- and 100-mm depths to determine BD and θ by oven-drying the samples at 105℃ for 24 h. Measurements were made from DOY 202 to 234 in 2020.

3. Model development

3.1. Variations of h and ρ with θ

Fig. 1 presents the *h*(θ) and ρ(θ) curves of a sand soil during a drying process, which was reported by Weerts et al. (2001). In the unsaturated domain (i.e., within the θ range of 0–0.28 m^3 m^{-3}), both *h* and ρ increased nonlinearly with soil drying, but showed different trends with respect to soil water content. We divide the complete drying process into three stages (I, II, and III) by considering the interactions of water with soil solids.

At the wetting end (i.e., stage I) where the soil system is close to saturation, water loss occurs at the soil surface, and the rate of water loss is determined mainly by the atmospheric evaporative demand, with negligible effects from soil capillary and surface forces on water

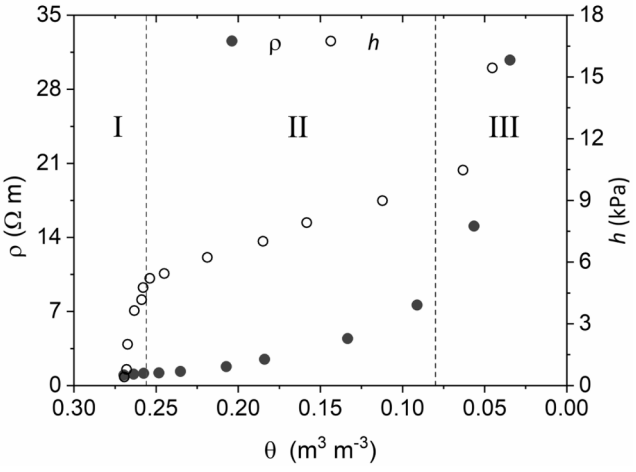

Fig. 1. A typical example showing the variation of electrical resistivity (ρ) and soil water suction (*h*) with water content (θ) on a sand soil during a drying process (original data were from Fig. 3 in Weerts et al., 2001 with units converted). Regions I, II, and III indicate the three stages of the soil drying process.

molecules. When the free surface water is depleted, evaporative water shifts to soil water, which is associated with soil solids and pore systems due to surface and capillary forces. When θ is decreased from about saturation to the air entry suction, the h value increases dramatically from 0 to about 5 kPa (Fig. 1). However, the ρ values are low (about 1 Ω m) and hardly change at this stage because electrical charges move freely with water (Rhoades et al., 1976; Rhoades et al., 1989). For some soils, a slight ρ decrease may occur due to the dissolution of the adsorbed and precipitated ions from the soil solid phase (Pozdnyakov et al., 2006).

Stage II starts off when the location of evaporation shifts from the surface to the subsurface where the mobility of water molecules is constrained interactively by capillary and adsorptive forces. Capillary force plays a key role in the relatively wet range, while adsorptive force dominates in the moderately dry range. In response, the electrical charges flow primarily with capillary water at higher θ values but shift to film water dominated mode later. Thus, at stage II, the fraction of capillary water decreases gradually, and the fraction of film water increases progressively (Pozdnyakov et al., 2006), which lead to gradual increases in h and ρ.

As the soil continues to dry, water films decrease and water molecules are bound strongly by intermolecular forces due to Van der Waals forces, water-solute-clay interactions and electrostatic interactions between solid surfaces and water dipoles (Pozdnyakov et al., 2006; Lu et al., 2015). At this stage (i.e., stage III), with the decrease of water content, both ρ and h increase exponentially because the water molecules and solutes adsorbed on the soil mineral surfaces are essentially immobile.

In this study, our analysis focuses on the h and ρ relationship in the θ range at suctions greater than the air entry value (i.e., stages II and III).

3.2. Model development

In this study, the Gardner (1970) model is used to describe the SWRC, i.e., the soil water content θ as a function of water suction h,

$$\theta = ah^{b} \tag{1}$$

where a and b are model parameters.

For unsaturated soils, the electrical resistance ρ depends on the volumetric fractions of soil solid, water and air phases due to the different abilities of each phase to conduct electricity. Archie's second law (Archie, 1942) has been applied to describe the relationship between ρ, porosity n and water saturation S of a soil,

$$\rho = d\rho_{w} n^{-m} S^{-c} \tag{2}$$

where ρ and ρ_w are the resistivities of the bulk soil and pore water (Ω m), respectively; d is a tortuosity factor that varies from 0.2 to 1.5 (Schön, 1996); S is the degree of water saturation; m is a cementation exponent, which is related to the electrical tortuosity of the soil; and c is a saturation exponent related to soil wettability, with values normally in the range of 1.8–2.2 (Schön, 1996; Revil, 1999).

For most soils, parameters m and c fall approximately in the same range (Nouveau et al., 2016). Thus, we assume that m and c take the same value. Then, by definition,

$$n^{-m} S^{-c} = (nS)^{-m} = \theta^{-m} \tag{3}$$

Combining Eqs. [2] and [3], we have,

$$\rho_{r} = \frac{\rho}{\rho_{w}} = d\theta^{-m} \tag{4}$$

where ρ_r is the formation factor.

For convenience of data analysis, we take the logarithms of ρ_r, h and θ. Then, Eq. [1] becomes,

$$log(h) = \frac{1}{b} log(\theta) - \frac{log a}{b} \tag{5}$$

and Eq. [4] becomes,

$$log(\rho_{r}) = -m\log(\theta) + log d \tag{6}$$

By incorporating Eq. [6] into Eq. [5], we obtain the following relationship between h and ρ_r,

$$\log(h) = -\frac{1}{bm} log(\rho_{r}) + \frac{1}{b}\left[\frac{1}{m} log d - log a\right] \tag{7}$$

By taking $A = -\frac{1}{bm}$ and $B = \frac{log d}{bm} - \frac{log a}{b}$, Eq. [7] is simplified as,

$$log(h) = A log(\rho_{r}) + B \tag{8}$$

Thus, there is a linear relationship between log(h) and log (ρ_r). For a specific soil, once the parameters A and B (or a and d, b, and m) are determined (which will be discussed in the following section), Eq. [8] can be applied to estimate h from ρ_r measurements, or vice versa.

3.3. Determination of ρ_w

The electrical resistivity of pore water ρ_w is required to estimate the bulk electrical resistivity ρ from the formation factor ρ_r. Fu et al. (2021b) developed a general form of Archie's model to estimate soil σ (or 1/ρ, the reciprocal of ρ),

$$\sigma = \sigma_{dry} + \sigma_{w}\theta^{w} + \sigma_{s} n \theta^{w-1} \tag{9}$$

where σ_{dry} is the σ value of the dry soil (dS m^{-1}), σ_w is the electrical conductivity of the water phase (dS m^{-1}), σ_s is soil surface conductivity (dS m^{-1}), and w is the phase exponent of pore water.

The value of w can be obtained by fitting Eq. [9] to a measured σ-θ dataset. Fu et al. (2021b) obtained a constant w value of 2 based on calibration using σ and θ datasets from 15 soils. Our analysis on soils 1–8 (Table 1), however, showed that the coarse-textured soils generally had lower w values than those for fine-textured soils (Fig. 2). Following Lu et al. (2007), we classified the soils into fine-textured and coarse-textured groups using a sand fraction (f_{sa}) of 0.40. Soils 1–4, the coarse-textured group with f_{sa} greater than 0.40, had a mean w value of 0.98. Soils 5–8, the fine-textured group with f_{sa} equal or lower than 0.40, had a w value of 1.97. Considering that 1.97 was close to the value of 2 in Fu et al. (2021b), we set the constant w to 2 for fine-textured soils.

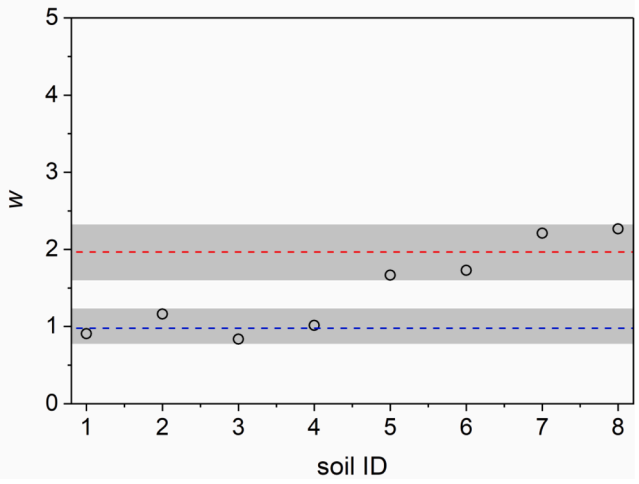

Fig. 2. The phase exponent (w) for soils 1–8. The lower dashed line represents the mean value for soils 1–4 (sand fraction ≥ 40%), and the upper dashed line represents the mean value for soils 5–8 (sand fraction < 40%). The two shadowed areas represent the ranges of w values for soils 1–4 and soils 5–8, respectively.

Accordingly, we rounded the w value of 0.98 to 1 for coarse-textured soils. Thus, by anchoring σ values at saturation and dry condition, σ_w (the reciprocal of ρ_w) can be calculated as,

$$\rho_w = \frac{1}{\sigma_w} = \frac{1}{\frac{\sigma_{sat}-\sigma_{dry}}{n^w} - \sigma_s} \quad (10)$$

where σ_{sat} is the saturated electrical conductivity (dS m^{-1}).

In Eqs. [9] and [10], the electrical conductivity of soil solids σ_s relates to soil cation exchange capacity, and thus to clay content (Waxman and Smits, 1968; Rhoades et al., 1989; Fu et al., 2021a). Rhoades et al. (1989) proposed an empirical equation to estimate σ_s from clay content based on the results from 6 soils with clay content ranging from 8% to 40%,

$$\sigma_s = 2.30 f_{cl} - 0.021 \quad [11]$$

Thus, Eq. [9] can be rewritten as,

$$\rho_w = \frac{1}{\sigma_w} = \frac{1}{\frac{\sigma_{sat}-\sigma_{dry}}{n^w} - 2.30 f_{cl} + 0.021} \quad (12)$$

3.4. Determination of model parameters A and B

We used the h and ρ measurements made on soils 1 to 8 to determine parameters A and B in the proposed model (Eq. [8]). These soils included a range of texture (from sand to clay loam), water content (from 0.06 to 0.60 m^3 m^{-3}), and bulk density (from 1.05 to 1.58 Mg m^{-3}) (Table 1). The log(ρ_r) values varied from 0 to 1, and log(h) varied from 0 to 3. For all 8 soils, the log(h) values increased approximately linearly with log (ρ_r) (Fig. 3). By fitting Eq. [8] to the data, we obtained A as the slope and B as the intercept of the regression lines. In general, the coarse-textured soils (soils 1–4) had relatively low A values and positive B values, while the fine-textured soils (soils 5–8) had relatively large A values and negative B values (Table 2). Accordingly, the B/A ratios were positive for soils 1–4 and negative for soils 5–8.

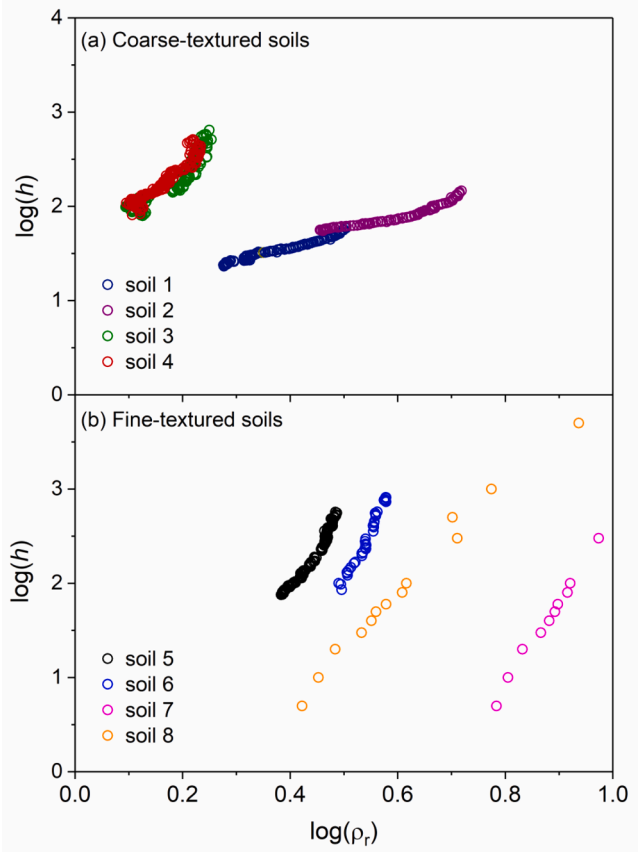

Fig. 3. Variations of the logarithm of soil water suction (log(h)) versus the logarithm of the formation factor (log(ρ_r)) for soils 1–8.

It has been reported that the magnitudes of h and/or ρ depend largely on soil specific surface area, which is related closely to the soil silt (f_{si}) and clay (f_{cl}) fractions (Lu et al., 2015). In addition, h and ρ vary with soil porosity n, a key indicator of soil structure. Thus, we further examined the functional relationships between A, B/A, $(f_{cl}+f_{si})$ and porosity n. Our analysis revealed that parameter A increased linearly with $(f_{cl}+f_{si})^n$, while the ratio B/A decreased linearly with $(f_{cl}+f_{si})^n$ (Fig. 4), and the relationships can be described with the following functions,

$$A = 15.29(f_{si}+f_d)^n - 4.96 \quad R^2 = 0.92^{**} \quad (13)$$

$$B/A = -2.89(f_{si}+f_{cl})^n + 2.16 \quad R^2 = 0.92^{**} \quad (14)$$

Thus, once f_{si}, f_{cl}, n, σ_{sat}, σ_{dry} and ρ data are available, h values can be estimated directly by using Eqs. [8]-[14].

4. Model evaluation

We evaluated the performance of the new model to estimate h by using independent measurements on soils 9–11. We also compared the performance of the new model against that of the Fu et al. (2021a) model. To our knowledge, the Fu et al. (2021a) model is the only available function that relates h and ρ. Fu et al. (2021a) applied the following equations to estimate the parameters of the van Genuchten (1980) model,

$$\theta = \theta_r + (\theta_s - \theta_r)\left[\left(1+(\alpha h)^l\right)^{1-\frac{1}{l}}\right] \quad (15)$$

$$\theta_r = (0.33 f_{cl} + 0.007)\frac{BD}{\rho_w} \quad (16)$$

$$\theta_s = 1 - \frac{BD}{\rho_s} \quad (17)$$

$$\frac{\sigma - \sigma_{dry}}{\sigma_{sat} - \sigma_{dry}} = \frac{\left[1-\left(1-S_e^{l/(l-1)}\right)^{(1-1/l)}\right]^2}{1-\left(1-S_e^{1/p}\right)^p} S_e^{\beta+1} \quad (18)$$

$$\left| -l(\theta_s-\theta_r)\left[1+\frac{l}{l-1}\right]^{\left(\frac{1}{l}-2\right)} \right| = \frac{\theta_s - \left((\theta_s-\theta_r)\left[1+\frac{1}{l-1}\right]^{\left(\frac{1}{l}-1\right)} + \theta_r\right)}{ln\left|\frac{1}{\alpha}\left(\frac{l}{l-1}\right)^{(1-l)}\right| - ln\left|\left(\frac{0.3}{\alpha}\right)^{1.26}\right|} \quad (19)$$

where θ_r and θ_s are residual and saturated water contents (m^3 m^{-3}), respectively, S_e is effective saturation, l (>1) is a pore-size distribution parameter, α (>0, cm^{-1}) is related to the inverse of the air entry suction, p is analogous to m, β is an empirical pore-tortuosity factor that is

Table 2
Parameters A, B and B/A obtained by fitting Eq. [8] to the measured log(h) and log(ρ_r) values on soils 1–8.

Soil ID	Texture	BD (Mg m^{-3})	A	B	B/A
1	sand	1.58	1.04	1.15	1.09
2	loamy sand	1.57	1.34	1.19	0.88
3	sandy loam	1.40	4.17	1.84	0.44
4	sandy loam	1.30	4.73	1.54	0.33
5	clay loam	1.20	8.10	−1.27	−0.16
6	silt loam	1.30	11.22	−3.60	−0.32
7	silt loam	1.25	5.65	−1.49	−0.26
8	clay loam	1.20	8.65	−6.38	−0.74

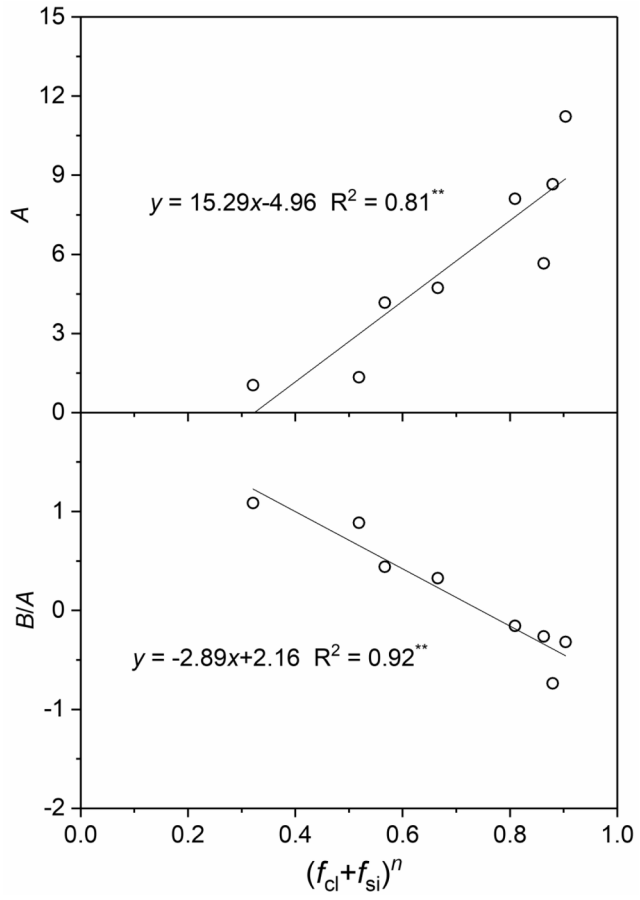

Fig. 4. Dependence of parameter A and parameter B/A on $(f_{cl} + f_{si})^n$ in soils 1–8. The symbols represent the fitted A and B/A values shown in Table 2. The lines are the linear regression results. R^2 represents the coefficient of determination.

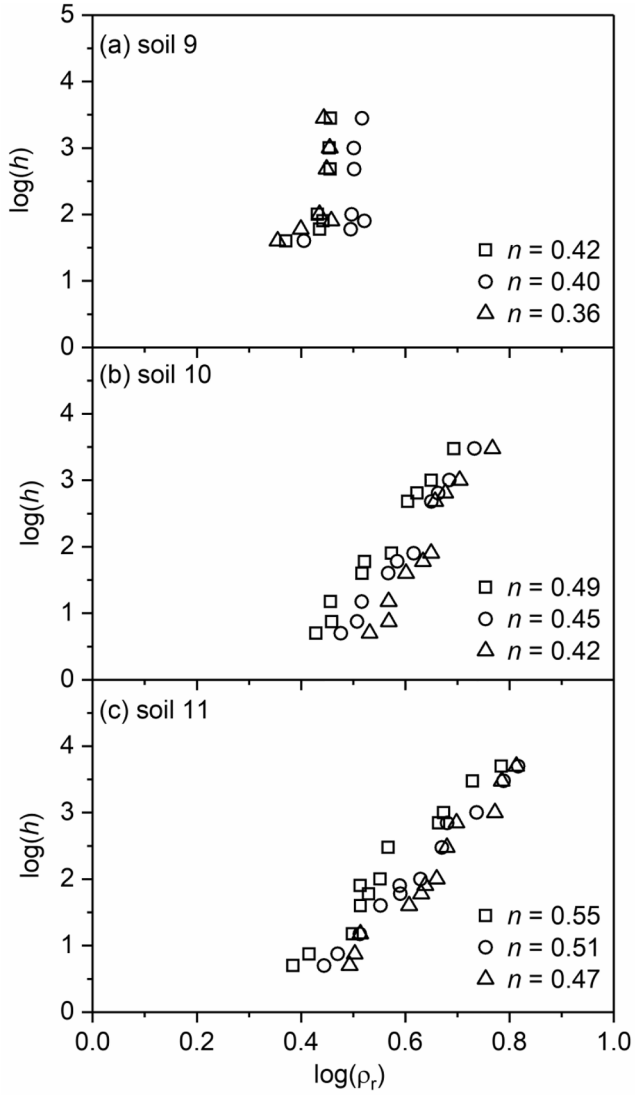

Fig. 5. The relationship between soil water suction (expressed as log(h)) and the formation factor (expressed as log(ρ_r)) for soils 9–11 at various porosities (n).

suggested as −1.28 for sand and −6.97 for loam and clay loam (Schapp and Leij, 2000), σ_{res} is the soil electrical conductivity at residual water content.

To determine parameter σ_{res}, we first obtained the SWRC functions of soils 9–11 by fitting the Gardner model to measured data, and then assumed the water content at $h = 1500$ kPa to be θ_r . Finally, σ_{res} was estimated from TDR measurements on soil columns repacked at θ_r and selected BD values.

Root mean square errors (RMSE) and bias of the estimations were calculated with respect to the measured values,

$$\mathrm{RMSE} = \sqrt{\frac{\sum (h_i - h_j)^2}{M}} \tag{20}$$

$$\mathrm{bias} = \frac{\sum (h_i - h_j)}{M} \tag{21}$$

where M is the number of measurements, h_i is the measured h value, and h_j is the estimated h value.

4.1. Model evaluation using measurements on repacked soil columns

Fig. 5(a)-5(c) present the measured log(h) versus log(ρ_r) data on repacked samples of soils 9–11. Irrespective of soil texture and porosity, the log(h) values increased linearly with log(ρ_r). For soil 9, log(h) increased linearly with log(ρ_r) in the wet range (log(h) < 2) but hardly changed in the dry range (log(h) > 2) (Fig. 5(a)). This was caused by the fact that in the dry state (i.e., log(h) > 2), all the water molecules were tightly bound onto mineral surfaces, and the electrical resistance of the bulk soil was at the maximum value.

Fig. 6(a)-6(c) compare the performance of the new model (Eqs. [8]-[14]) to that of the Fu et al. (2021a) model (Eqs. [15]-[19]) using the measurements from repacked columns of soils 9–11. For the sand (soil 9), the comparison between observed and estimated log(h) data was limited in the wet range (log(h) < 2) because the measured ρ values showed no response to h in the dry range (Fig. 5a). In general, the Fu et al. (2021a) model gave accurate log(h) estimates on soil 9 with a RMSE of 0.15 kPa (Fig. 6a). For the new model, although the estimated data related well with the measured ones, it significantly overestimated log(h) with a RMSE of 0.85 kPa. The overestimation might be caused by the limitations of calibration dataset, which was dominated by data from loam and clay soils, and only one sand was covered. Further studies are required to improve the model performance on sandy soils.

On soils 10–11, data from the new model and the Fu et al. (2021a) model generally distributed around the 1:1 lines (Fig. 6b and 6c), indicating that both models provided relatively accurate results on the fine-texture soils. However, the RMSEs of the new model (0.21 for soils 10 and 0.16 kPa for 11), which were lower than the corresponding RMSEs (0.28 kPa and 0.21 kPa) of the Fu et al. (2021a) model (Table 3), which was especially evident for soil 10 at higher bulk densities. These

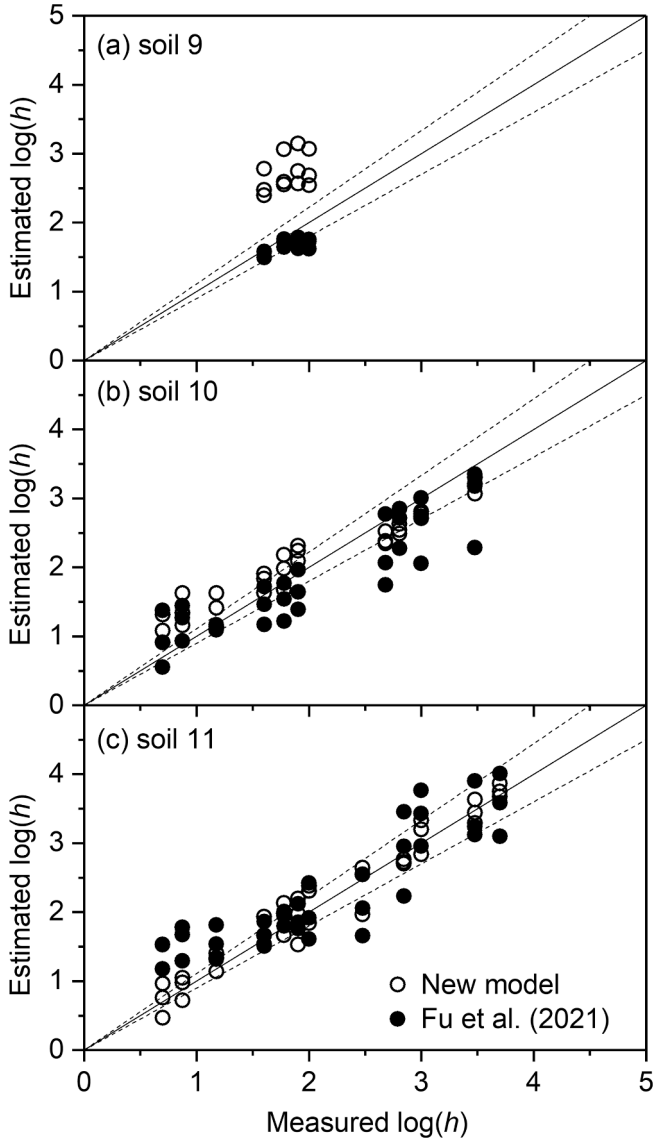

Fig. 6. Comparisons of the new model and Fu et al. (2021) model estimations to measured soil water suction (expressed as log(*h*)) for soils 9–11. The solid lines are the 1:1 lines, and the dashed lines are the 10% error lines.

Table 3
Root mean square errors (RMSEs) of the estimated soil water suction (*h*) values derived from the new model and from the Fu et al. (2021a) model for Soils 9–11 in repacked soil columns and for the field measurements.

	Soil ID	Texture	New model	Fu et al. (2021a)
				kPa
Laboratory study	9	sand	0.85	0.15
	10	silt loam	0.21	0.28
	11	clay loam	0.16	0.29
Field study	11	clay loam	0.23	–

deviations could be attributed to the limitation of the Fu et al. (2021a) model that assumed a common geometry factor controlling the flows of water and electrical current in soil pore space (Mualem and Friedman, 1991). When a soil is compacted, however, the total porosity *n* is decreased and the pore size distribution is altered, which resulted in a greater heterogeneity of the pore system. In response, the flow path of electrical current differs from that of water flow: As *n* decreases, electrical current transmission through the solid path and solid–liquid path becomes significant, resulting in a greater geometry factor for electrical current transmission than that for water flow. Thus, the model assumption of a common geometry factor yields a reduced geometry factor for electrical current, a greater *l* value (Eq. [18]), and finally an underestimated log(*h*). Thus, further studies are required to improve the Fu et al. (2021a) model by accounting for changes in soil bulk density.

4.2. Model evaluation using in situ field measurements

Field dynamics of ρ and *h* at the 5-cm depth were monitored on soil 11 through DOY 202 to 234 in 2020. The BD was about 1.13 Mg m^{-3}, and the θ, *h* and ρ values varied from 0.12 to 0.47 m^3 m^{-3}, 0.81 to 959 kPa, and 36.1 to 94.8 Ω m, respectively. Fig. 7(a) and 7(b) show the temporal values for θ, *h*, ρ and rainfall during the entire measurement period. It was clear that the *h* and ρ values decreased rapidly with rainfall events and then gradually increased as the soil dried. Using DOY 217–224 as an example, in response to the 24.4-mm rainfall on DOY 216, θ increased from 0.19 m^3 m^{-3} on DOY 216 to 0.39 m^3 m^{-3} on DOY 217. At the same time, *h* (from 481 to 5.6 kPa) and ρ (from 75.9 to 38.3 Ω m) decreased sharply. Subsequently, θ decreased gradually from 0.39 m^3 m^{-3} on DOY 217 to 0.12 m^3 m^{-3} on DOY 224, during which ρ and *h* increased dramatically: *h* increased by 558 kPa (from 5.6 to 564 kPa) and ρ increased by 45.4 Ω m (from 38.3 to 83.7 Ω m).

The estimated log(*h*) values were obtained from measured ρ values using Eq. [8]. The input parameter σ_{sat} was the in situ measured σ value at saturation, and σ_{dry} was approximated from the measured σ value of a repacked soil column at a dry condition with the same BD. Comparisons between the estimated and measured log(*h*) values showed that most of the data were distributed randomly along the 1:1 line, about 70% of the data were within the 10% error lines (Fig. 8), and the RMSE of the model estimates was 0.23 kPa (Table 3). Overall, the new model not only successfully captured the temporal variability in field log(*h*) values, but also provided acceptable *h* values. Nonetheless, some data points deviated from the 1:1 line considerably, especially in the log(*h*) range of

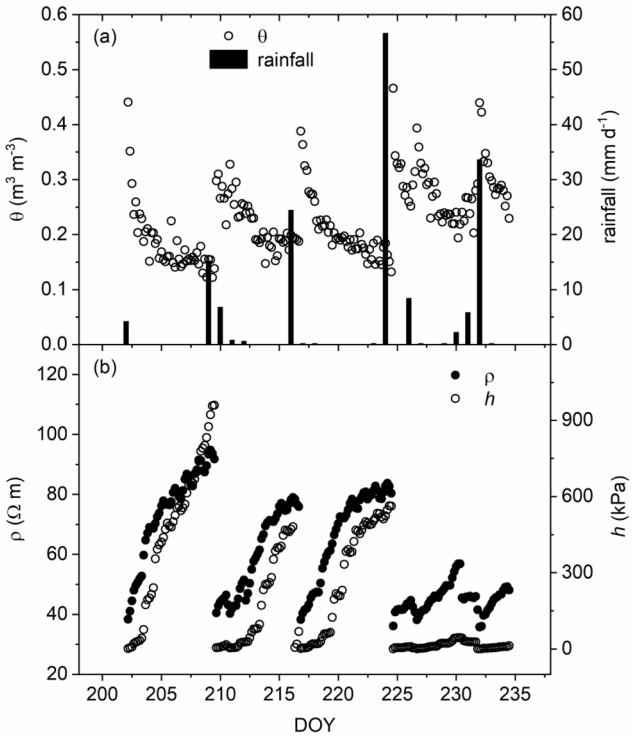

Fig. 7. (a) Temporal variations of soil water content (θ), rainfall and (b) soil electrical resistivity (ρ), water suction (*h*) of soil 11 at the 5-cm depth from DOY 202 to 234, 2020.

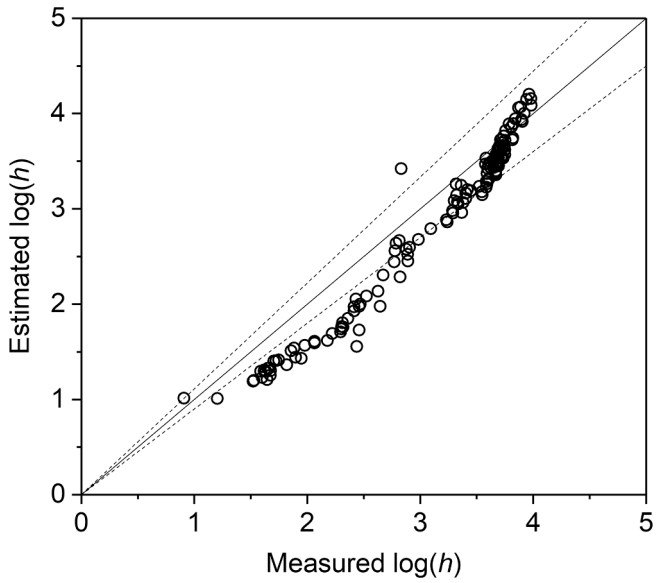

Fig. 8. In situ log(h) estimated values vs. measured log(h) values using the new model for soil 11 at the 5-cm depth. The solid line is the 1:1 line, and the dashed lines are the 10% error lines.

1.5–3.0 where h was overestimated. Several factors might have contributed to the uncertainties. First, under field condition, the h readings from the TensioMark sensor are sensitive to soil temperature change, soil-sensor contact, and structural changes due to soil disturbance and swelling/shrinking during wetting/drying (Bruand and Cousin, 1996; Sun et al., 2009; Bonder et al., 2013; Zhang et al., 2017). Secondly, the relationship between soil electrical conductivity and water suction displays a strong hysteresis effect (Bottraud and Rhoades, 1985), which inevitably manifests under field conditions. Additionally, the functions and parameters of the new model were developed based on the measurements made in soil columns representing 8 soils, and thus have inherent limitations for field applications.

4.3. Limitations of the new model

There are some limitations to the new empirical h-ρ relationship. First, the Gardner (1970) model takes the form of a power function, which fails to reflect the dramatic h decreases in the near saturated range when h is lower than the air entry value. Also, the log(ρ_r) data (from soils 1–8) used to develop the new model were in the range between 0 and 1. Thus, the new model is only applicable in the θ range where h values are greater than the air entry value and the log(ρ_r) values are less than 1. Secondly, there are reports that σ_s is affected by the mobility of cations in the electrical double layer, porosity, and cation exchange capacity (Revil, 2012, 2013). Yet this study only considered the effect of f_{cl} on σ_s. Inaccurate σ_s results causes errors in the estimated parameters A and B, which then transfer to erroneous h data. Thirdly, under field conditions, soil water suction is strongly affected by hysteresis and temperature variation, which are neglected in this study. Finally, our validation results indicate that on the sand soil (soil 9), the estimated log(h) values were generally greater than the measured values. Further research is required to improve the model performance in coarse-textured soils.

It should be noted that in practice, the errors in h estimates will be propagated to related parameters. For example, the uncertainties of h estimates will give inaccurate SWRC values because a 5% error in measured ρ values will transfer to a 0–68% error in the modelled h values, depending on soil texture. In our field data, the h value estimates have an average deviation of 12% from the measured ones, which causes a 30% error in θ estimates when the van Genuchten model (Eq. [15]) is used to describe the SWRCs. These uncertainties can affect applications such as irrigation scheduling and modelling studies of water and solute transport in soils.

5. Conclusion

In this study, we examined the functional relationship between soil water suction h and electrical resistivity ρ. Theoretical analysis and experimental results showed that h and ρ were closely correlated for h values greater than the air entry value and log(ρ_r) values less than 1. A new h model (Eqs. [8]-[14]) was developed based on Archie's second law and the Gardner (1970) soil water retention model. The input parameters of the new model included soil texture, porosity n, ρ, phase exponent of pore water w, and electrical conductivities of saturated (σ_{sat}) and dry soil (σ_{dry}). Evaluations of the new h-ρ model using measurements on repacked soil samples and in situ field data showed that the new model provided acceptable h estimates. Additional studies are required to test the new model in a range of soils representing various field conditions, and to enhance the model performance on coarse-textured soils.

Declaration of Competing Interest

The authors declare that they have no known competing financial interests or personal relationships that could have appeared to influence the work reported in this paper.

Acknowledgement

This research was supported by the National Natural Science Foundation of China (41977011), the 2115 Talent Development Program of China Agricultural University (1191-00109011), and the U.S. National Science Foundation (2037504) and USDA-NIFA Multi-State Project 4188.

References

Al-Moadhen, M.M., 2019. Hydraulic, Thermal and Electrical Conductivities of Composite Soils. University of Leeds, Ph.D. diss.
Archie, G.E., 1942. The electrical resistivity log as an aid in determining some reservoir characteristics. Trans. Am. Inst. Mining Metallurgical Eng. 146, 54–62.
Bittelli, M., Flury, M., 2009. Errors in water retention curves determined with pressure plates. Soil Sci. Soc. Am. J. 73 (5), 1453–1460.
Bonder, G., Scholl, P., Loiskandl, W., Kaul, H.P., 2013. Environmental and management influences on temporal variability of near saturated soil hydraulic properties. Geoderma 204–205 (Complete), 120–129.
Børgesen, C.D., Iversen, B.V., Jacobsen, O.H., Schaap, M.G., 2008. Pedotransfer functions estimating soil hydraulic properties using different soil parameters. Hydrol. Process. 22 (11), 1630–1639.
Bottraud, J.-C., Rhoades, J.D., 1985. Referencing water content effects on soil electrical conductivity-salinity calibrations. Soil Sci. Soc. Am. J. 49 (6), 1579–1581.
Bruand, A., Cousin, I., Nicoullaud, B., Duval, O., Bégon, J.C., 1996. Backscattered electron scanning images of soil porosity for analyzing soil compaction around roots. Soil Sci. Soc. Am. J. 60 (3), 895–901.
Dane, J.H., Hopmans, J.W., 2002. Water Retention and Storage. p. 671-796. In J.H. Dane and G.C. Topp (ed.) Methods of Soil Analysis. Part. 4. Physical Methods. SSSA, Madison, WI.
Doussan, C., Ruy, S., 2009. Prediction of unsaturated soil hydraulic conductivity with electrical conductivity. Water Resour. Res. 45, W10408.
Flint, A.L., Flint, L.E., 2002. Particle Density. p. 229-240. In J.H. Dane and G.C. Topp (ed.) Methods of Soil Analysis. Part. 4. Physical Methods. SSSA, Madison, WI.
Friedman, S.P., 2005. Soil properties influencing apparent electrical conductivity: A review. Comput. Electron. Agric. 46 (1-3), 45–70.
Fu, Y., Horton, R., Heitman, J., 2021a. Estimation of soil water retention curves from soil bulk electrical conductivity and water content measurements. Soil Tillage Res. 209, 104948. https://doi.org/10.1016/j.still.2021.104948.
Fu, Y., Horton, R., Ren, T., Heitman, J.L., 2021b. A general form of Archie's model for estimating bulk soil electrical conductivity. J. Hydrol. 597, 126160. https://doi.org/10.1016/j.jhydrol.2021.126160.
Gardner, W.R., Hillel, D., Benyamini, Y., 1970. Post-irrigation movement of soil water. 1. Redistribution. Water Resour. Res. 6 (3), 851–861.
Gee, G.W., Or, D., 2002. Particle-size Analysis. p. 255-293. In J.H. Dane and G.C. Topp (ed.) Methods of Soil Analysis. Part. 4. Physical Methods. SSSA Book Ser. 5. SSSA, Madison, WI.

Gupta, S.C., Larson, W.E., 1979. Estimating soil water characteristics from particle size distribution, organic matter percent, and bulk density. Water Resour. Res. 15, 1633–1635.
Heimovaara, T.J., Focke, A.G., Bouten, W., Verstraten, J.M., 1995. Assessing temporal variations in soil water composition with time domain reflectometry. Soil Sci. Soc. Am. J. 59 (3), 689–698.
Karup, D., Moldrup, P., Tuller, M., Arthur, E., de Jonge, L.W., 2017. Prediction of the soil water retention curve for structured soil from saturation to oven-dryness. Eur. J. Soil Sci. 68 (1), 57–65.
Katz, A.J., Thompson, A.H., 1986. Quantitative prediction of permeability in porous rock. Phys. Rev. B 34 (11), 8179–8181.
Lu, N., Dong, Y.i., 2015. Closed-form equation for thermal conductivity of unsaturated soils at room temperature. J. Geotech. Geoenviron. Eng. 141 (6), 04015016. https://doi.org/10.1061/(ASCE)GT.1943-5606.0001295.
Lu, S., Ren, T., Gong, Y., Horton, R., 2007. An improved model for predicting soil thermal conductivity from water content at room temperature. Soil Sci. Soc. Am. J. 71 (1), 8–14.
Mohammadi, M.H., Vanclooster, M., 2011. Predicting the soil moisture characteristic curve from particle size distribution with a simple conceptual model. Vadose Zone J. 10 (2), 594–602.
Mualem, Y., Friedman, S.P., 1991. Theoretical prediction of electrical conductivity in saturated and unsaturated soil. Water Resour. Res. 27 (10), 2771–2777.
Naveed, M., Moldrup, P., Tuller, M., Ferrè, T.P.A., Kawamoto, K., Komatsu, T., de Jonge, L.W., 2012. Prediction of the soil water characteristic from soil particle volume fractions. Soil Sci. Soc. Am. J. 76 (6), 1946–1956.
Nelson, D.W., Sommers, L.E., 1982. Total Carbon, Organic Carbon, and Organic Matter. p. 539-579. In A.L. Page et al. (ed.) Methods of Soil Analysis. Part. 2. 2nd ed. Agron. Monogr. 9. ASA and SSSA, Madison, WI.
Niu, Q., Fratta, D., Wang, Y.-H., 2015. The use of electrical conductivity measurements in the prediction of hydraulic conductivity of unsaturated soils. J. Hydrol. 522, 475–487.
Nouveau, M., Grandjean, G., Leroy, P., Philippe, M., Hedri, E., Boukcim, H., 2016. Electrical and thermal behavior of unsaturated soils: experimental results. J. Appl. Geophys. 128, 115–122.
Perkins, K.S., 2011. Measurement and Modeling of Unsaturated Hydraulic Conductivity. p. 419-434. In L. Elango (ed.) Hydraulic Conductivity-Issues, Determination and Applications. In Tech Publishing.
Pham, H.Q., Fredlund, D.G., 2008. Equations for the entire soil-water characteristic curve of a volume change soil. Can. Geotech. J. 45 (4), 443–453.
Piegari, E., Di Maio, R., 2013. Estimating soil suction from electrical resistivity. Nat. Hazards Earth Syst. Sci. 13 (9), 2369–2379.
Pozdnyakov, A.I., Pozdnyakova, L.A., Karpachevskii, L.O., 2006. Relationship between water tension and electrical resistivity in soils. Eurasian Soil Science. 39 (S1), S78–S83.
Purvance, D.T., Andricevic, R., 2000. On the electrical-hydraulic conductivity correlation in aquifers. Water Resour. Res. 36 (10), 2905–2913.
Ren, T., Noborio, K., Horton, R., 1999. Measuring soil water content, electrical conductivity, and thermal properties with a thermo-time domain reflectometry probe. Soil Sci. Soc. Am. J. 63 (3), 450–457.
Revil, A., 1999. Ionic diffusivity, electrical conductivity, membrane and thermoelectric potentials in colloids and granular porous media: a unified model. J. Colloid Interface Sci. 212 (2), 503–522.
Revil, A., 2012. Spectral induced polarization of shaly sands: influence of the electrical double layer. Water Resour. Res. 48, W02517.
Revil, A., 2013. Effective conductivity and permittivity of unsaturated porous materials in the frequency range 1 mHz-1GHz. Water Resour. Res. 49 (1), 306–327.
Rhoades, J.D., Raats, P.A.C., Prather, R.J., 1976. Effects of liquid phase electrical conductivity, water content, and surface conductivity on bulk soil electrical conductivity. Soil Sci. Soc. Am. J. 40 (5), 651–655.
Rhoades, J.D., Manteghi, N.A., Shouse, P.J., Alves, W.J., 1989. Soil electrical conductivity and soil salinity: new formulations and calibrations. Soil Sci. Soc. Am. J. 53 (2), 433–439.
Richards, B.G., 1965. Measurement of the free energy of soil moisture by the psychrometric technique using thermistors. In: Moisture Equilibria and Moisture Changes in Soils Beneath Covered Areas: A Symposium. Butterworths, Australia, pp. 39–46.
Romano, N., Hopmans, J., Dane, J.H., 2002. Suction Table. p. 692-698. In J.H. Dane and G.C. Topp (ed.) Methods of Soil Analysis. Physical Methods. SSSA Book Ser. 5 Part. 4. SSSA, Madison, WI.
Schaap, M.G., Leij, F.J., 1998. Using neural networks to predict soil water retention and soil hydraulic conductivity. Soil Tillage Res. 47, 37–42.
Schaap, M.G., Leij, F.J., 2000. Improved prediction of unsaturated hydraulic conductivity with the Mualem-van Genuchten model. Soil Sci. Soc. Am. J. 64 (3), 843–851.
Schön, J.H., 1996. Physical Properties of Rocks: Fundamentals and Principles of Petrophysics. Pergamon Press, New York.
Slater, L., Lesmes, D.P., 2002. Electrical-hydraulic relationships observed for unconsolidated sediments. Water Resour. Res. 38 (10), 31-1–31-13.
Stadler, A., Rudolph, S., Kupisch, M., Langensiepen, M., van der Kruk, J., Ewert, F., 2015. Quantifying the effects of soil variability on crop growth using apparent soil electrical conductivity measurements. Eur. J. Agron. 64, 8–20.
Sudduth, K.A., Kitchen, N.R., Wiebold, W.J., Batchelor, W.D., Bollero, G.A., Bullock, D. G., Clay, D.E., Palm, H.L., Pierce, F.J., Schuler, R.T., Thelen, K.D., 2005. Relating apparent electrical conductivity to soil properties across the north-central USA. Comput. Electron. Agric. 46 (1-3), 263–283.
Sun, Y., Lin, J., Lammers, P.S., Damerow, L., Hueging, H., Zhang, H., Sun, W., 2009. Predicting surface porosity using a fine-scale index of roughness in a cultivated field. Soil Tillage Res. 103 (1), 57–64.
Tian, Z., Kool, D., Ren, T., Horton, R., Heitman, J.L., 2018. Determining in-situ unsaturated soil hydraulic conductivity at a fine depth scale with heat pulse and water potential sensors. J. Hydrol. 564, 802–810.
Urish, D.W., 1981. Electrical resistivity-hydraulic conductivity relationships in glacial outwash aquifers. Water Resour. Res. 17 (5), 1401–1408.
van Genuchten, M.T., 1980. A closed-form equation for predicting the hydraulic conductivity of unsaturated soils. Soil Sci. Soc. Am. J. 44 (5), 892–898.
De Vita, P., Di Maio, R., Piegari, E., 2012. A study of the correlation between electrical resistivity and matric suction for unsaturated ash-fall pyroclastic soils in the Campania region (southern Italy). Environ. Earth Sci. 67 (3), 787–798.
Waxman, M.H., Smits, L.J.M., 1968. Electrical conductivities in oil-bearing shaly sands. J. Petrol. Sci. Eng. 8, 107–122.
Weerts, A.H., Kandhai, D., Bouten, W., Sloot, P.M.A., 2001. Tortuosity of an unsaturated sandy soil estimated using gas diffusion and bulk soil electrical conductivity. Soil Sci. Soc. Am. J. 65 (6), 1577–1584.
Weynants, M., Vereecken, H., Javaux, M., 2009. Revisiting Vereecken pedotransfer functions: introducing a closed-form hydraulic model. Vadose Zone J. 8 (1), 86–95.
Wösten, J.H.M., Lilly, A., Nemes, A., Le Bas, C., 1999. Development and use of a database of hydraulic properties of European soils. Geoderma 90 (3-4), 169–185.
Zhang, M., Lu, Y., Heitman, J., Horton, R., Ren, T., 2017. Temporal changes of soil water retention behavior as affected by wetting and drying following tillage. Soil Sci. Soc. Am. J. 81 (6), 1288–1295.
Zhang, P., Wu, Q., Jiang, G., Pu, Y., 2011. Relation between soil matrix potential changes and water conversion ratios during methane hydrate formation processes in loess. J. Nat. Gas Chem. 20 (2), 140–144.